THE JOURNAL OF BIOLOGICAL CHEMISTRY VOL. 289, NO. 48, pp. 33333–33342, November 28, 2014

Spatial Control of Proton Pump H,K-ATPase Docking at the Apical Membrane by Phosphorylation-coupled Ezrin-Syntaxin 3 Interaction*

Received for publication, May 12, 2014, and in revised form, October 8, 2014 Published, JBC Papers in Press, October 9, 2014, DOI 10.1074/jbc.M114.581280

Huijuan Yu[‡1], Jiajia Zhou[‡§1], Hirohide Takahashi[¶], William Yao[§2], Yuki Suzuki[¶], Xiao Yuan[‡], Shige H. Yoshimura[¶], Yin Zhang[‡‖], Ya Liu[‡], Nerimiah Emmett[§], Vincent Bond[§], Dongmei Wang[‡], Xia Ding[‖], Kunio Takeyasu[¶3], and Xuebiao Yao[‡4]

From the [‡]Anhui Key Laboratory for Cellular Dynamics and Chemical Biology, University of Science and Technology of China School of Life Science, Hefei, China 230027, [¶]Laboratory of Plasma Membrane, Graduate School of Biostudies, Kyoto University, Kyoto 606-8502, Japan, [§]Morehouse School of Medicine, Atlanta, Georgia 30310, and [‖]Graduate School, Beijing University of Chinese Medicine, Beijing 100086, China

Background: Polarized acid secretion in gastric parietal cells requires ezrin and its phosphorylation at Ser-66.
Results: Phosphorylation of Ser-66 induces ezrin conformational change, which enables ezrin to interact with syntaxin 3.
Conclusion: Conformational change of ezrin provides a spatial cue for apical trafficking of H,K-ATPase.
Significance: Ezrin conformation orchestrates the polarized vesicle trafficking in epithelial cells.

The digestive function of the stomach depends on acidification of the gastric lumen. Acid secretion into the lumen is triggered by activation of a cAMP-dependent protein kinase (PKA) cascade, which ultimately results in the insertion of gastric H,K-ATPases into the apical plasma membranes of parietal cells. A coupling protein is ezrin whose phosphorylation at Ser-66 by PKA is required for parietal cell activation. However, little is known regarding the molecular mechanism(s) by which ezrin operates in gastric acid secretion. Here we show that phosphorylation of Ser-66 induces a conformational change of ezrin that enables its association with syntaxin 3 (Stx3) and provides a spatial cue for H,K-ATPase trafficking. This conformation-dependent association is specific for Stx3, and the binding interface is mapped to the N-terminal region. Biochemical analyses show that inhibition of ezrin phosphorylation at Ser-66 prevents ezrin-Stx3 association and insertion of H,K-ATPase into the apical plasma membrane of parietal cells. Using atomic force microscopic analyses, our study revealed that phosphorylation of Ser-66 induces unfolding of ezrin molecule to allow Stx3 binding to its N terminus. Given the essential role of Stx3 in polarized secretion, our study presents the first evidence in which phosphorylation-induced conformational rearrangement of the ezrin molecule provides a spatial cue for polarized membrane trafficking in epithelial cells.

The functions of an epithelium depend on the polarized organization of its individual epithelial cells. The acquisition of a fully polarized phenotype involves a cascade of complex events including cell-cell adhesion, assembly of a lateral cortical complex, reorganization of the cytoskeleton, and polarized targeting of transport vesicles to the apical and basolateral membranes (1).

Ezrin is an actin-binding protein of the ezrin/radixin/moesin (ERM)[5] family of cytoskeleton-membrane linker proteins (2). Within the gastric epithelium ezrin has been localized exclusively to parietal cells and primarily to the apical canalicular membrane of these cells (3, 4). Our previous studies showed that gastric ezrin is co-distributed with the β-actin isoform *in vivo* (5) and preferentially bound to the β-actin isoform *in vitro* (6). It was postulated that ezrin couples the activation of protein kinase A to the apical membrane remodeling associated with parietal cell secretion (3, 7). In fact we have mapped the PKA phosphorylation site on ezrin and demonstrated the importance of the phospho-regulation of ezrin in gastric acid secretion (3). Using mouse genetics, Tamura (8) demonstrated that knock-down ezrin in stomachs to $<5\%$ of the wild type levels results in severe achlorhydria. In these parietal cells, H,K-ATPase-containing tubulovesicles failed to fuse with the apical membrane, suggesting an essential role of ezrin in tubulovesicle docking. However, it is still not clear how ezrin links the apical targeting of H,K-ATPase-containing tubulovesicle to the remodeling of apical membrane and cytoskeleton during the parietal cell activation.

Soluble *N*-ethylmaleimide-sensitive factor attachment protein receptors (SNAREs) are crucial for vesicle fusion. The three SNARE proteins form a four-helical bundle, the SNARE complex, which mediates membrane fusion (9). Our recent studies demonstrate the functional significance of Stx3 (10), VAMP2 (11), and

* This work was supported, in whole or in part, by National Institutes of Health Grants CA164133, DK56292, and G12RR03034. This work was also supported by Chinese 973 Projects 2012CB945002, 2012CB917204, and 2010CB912103, MOST 2009DFA31010, Ministry of Education 20113402130010, Anhui Project 08040102005, Chinese Natural Science Foundation Grants 31320103904, 31430054, 31271518, 91313303, 91129714, 81270466, and 31301105.
We dedicate this work to late Professor John G. Forte who discovered proton pump H,K-ATPase and founded the field of gastric parietal cell biology.
[1] Both authors contributed equally to this work.
[2] An American Digestive Health Foundation Student Research Fellow.
[3] To whom correspondence may be addressed. E-mail: takeyasu@kyoto.ac.jp.
[4] To whom correspondence may be addressed. E-mail: yaoxb@ustc.edu.cn.

[5] The abbreviations used are: ERM, ezrin/radixin/moesin; AP, aminopyrine; MEM, minimal essential medium; SLO, Streptolysin O; AFM, atomic force microscopy; MBP, maltose-binding protein.

SNAP25 (12) in the parietal cell exocytosis. Despite demonstration of the functional importance of Stx3 in parietal cell secretion (13, 14), it is still unclear how Stx3 facilitates the docking tubulovesicular membrane at the apical membrane.

The crystal structure of a dormant ezrin FERM-tail complex reveals that the FERM domain has three compact lobes including an integrated PTB-PH-EVH fold, with the C-terminal segment bound as an extended peptide masking a large surface of the FERM domain (15–17). Here we show that phosphorylation of Ser-66 unfolds the three compact lobes of the FERM domain and this conformational change enables association of Stx3 with ezrin. Thus, our study provides novel insight into the spatial control of H,K-ATPase docking by phosphorylation-coupled ezrin-Stx3 interaction in parietal cells.

MATERIALS AND METHODS

Isolation of Gastric Glands and Aminopyrine (AP) Uptake Assay—Gastric glands were isolated from New Zealand White rabbits as modified by Yao *et al.* (5). Briefly, the rabbit stomach was perfused under high pressure with PBS (2.25 mM K_2HPO_4, 6 mM Na_2HPO_4, 1.75 mM NaH_2PO_4, and 136 mM NaCl) containing 1 mM $CaCl_2$ and 1 mM $MgSO_4$. The gastric mucosa was scraped from the smooth muscle layer, minced, and then washed twice with MEM buffered with 20 mM HEPES, pH 7.4 (HEPES-MEM). The minced mucosa was then digested with 15 mg of collagenase (Sigma). Intact gastric glands were collected from the digestion mixture for 20–25 min and then washed 3 times in HEPES-MEM. In all subsequent gland experiments (AP uptake assay) glands were resuspended at 5% cytocrit (v/v) in the appropriate buffer for final assay.

Stimulation of intact and Streptolysin O (SLO)-permeabilized rabbit gastric glands was quantified using the AP uptake assay as described by Ammar *et al.* (20). Briefly, intact glands in HEPES-MEM were washed 2 times by settling at 4 °C in ice-cold K buffer (10 mM Tris base, 20 mM HEPES acid, 100 mM KCl, 20 mM NaCl, 1.2 mM $MgSO_4$, 1 mM NaH_2PO_4, and 40 mM mannitol, pH 7.4). SLO was added to a final concentration of 1 μg/ml, and the glands (at 5% cytocrit) were mixed by inversion and then incubated on ice for 10 min. The glands were then washed twice with ice-cold K buffer to remove unbound SLO whereas the permeabilization was initiated by incubating gland suspension at 37 °C in K buffer solution containing 1 mM pyruvate and 10 mM succinate.

To evaluate the function of Stx3-ezrin^{S66D} interaction in parietal cell activation, we generated recombinant deletion Stx3$^{1-147}$ and Stx3$^{147-180}$ mutants in bacteria. Briefly, GST-fusion ezrin and its mutants were expressed in BL21 (DE3) bacteria and purified as described (3). The fusion proteins were then eluted in PBS containing 10 mM glutathione and then applied to a gel filtration column (Econ-Pac 10 DG; Bio-Rad) to remove glutathione and exchange PBS buffer for K^+ buffer. Protein concentrations were determined by the Bradford assay (22).

Cell Culture and Transfection—Primary cultures of gastric parietal cells from rabbit stomach were produced and maintained as described (3). Separate cultures of parietal cells were transfected with plasmids encoding GFP-tagged wild type ezrin and/or deletion mutants using Lipofectamine 2000 (Invitrogen) according to the manufacturer's instructions. Briefly, 1 μg of DNA was incubated in 600 μl of Opti-MEM (antibiotic-free), whereas 6 μl of Lipofectamine 2000 was added and left at room temperature for 25 min. The cultured parietal cells (~3% cytocrit; 6-well plates) were washed once with Opti-MEM. The DNA-lipid mix was added to the plates and incubated for 4 h followed by replacement of 1.5 ml of medium B. The transfected cells were then maintained in culture at 37 °C until used for protein expression, partition, immunoprecipitation, or immunofluorescence.

Infection of culture parietal cells with adenoviral mCherry-ezrin, mCherry-ezrin^{S66A}, and mCherry-ezrin^{S66D} was described previously (11, 12, 22). The infection efficiency and level of various ezrin expression exhibit no difference.

Preparation of Gastric Subcellular Fractions—Gastric subcellular fractions were prepared according to Yao *et al.* (5). All fractionation procedures were performed under ice-cold conditions. Briefly, the treated glands were rinsed once in homogenizing buffer containing 125 mM mannitol, 40 mM sucrose, 1 mM EDTA, and 5 mM PIPES-Tris (pH 6.7) and homogenized with a very tightly fitting Teflon pestle. The homogenate was centrifuged to produce a series of pellets: PO, 40 × *g* for 5 min (whole cells and debris); P_1, 4,000 × *g* for 10 min (plasma membrane-rich fraction); P_2, 14,500 × *g* for 10 min; P_3, 100,000 × *g* for 60 min (microsomes); and S_3, supernatant (cytosol). The pellets were resuspended in medium containing 300 mM sucrose, 0.2 mM EDTA, and 5 mM Tris (pH 7.4). The protein concentration in each individual subcellular fraction was assayed using bovine serum albumin as a standard (6).

Affinity Purification of Ezrin and Phosphatase Treatment—To characterize the histamine-elicited protein interaction between ezrin and Stx3, anti-ezrin antibody 6H11 affinity matrix was prepared as by Yao *et al.* (19). Briefly, the precipitate of ascites containing 6H11 was dialyzed against distilled water and 0.1 M HEPES, pH 8.0. The beads were gently mixed with 6H11 for 4 h at 4°C. The 6H11-coupled beads were washed with PBS then incubated with 1 M ethanolamine, pH 8.0, for 1 h to block excess un-reacted *N*-hydroxysuccinimide groups. The affinity column was stored at 4°C in PBS containing 0.1% NaN_3. Before each run the column was washed with elution buffer and re-equilibrated with PBS before applying gastric membrane extracts.

The gastric membrane fraction from histamine-stimulated preparation containing large organelles including apical plasma membrane fragments enriched in ezrin was extracted with extraction buffer containing 0.25% Triton X-100, 200 mM NaCl, 1 mM EGTA, 20 mM Tris-Cl, pH 7.4, and protease inhibitor mixture (Sigma) on ice for 30 min and centrifuged at 20,000 × *g* for 20 min. Aliquots of the supernatant were mixed by gentle rotation for 2 h at 4 °C with affinity matrix coupled with anti-ezrin antibody. To examine the protein interaction dependent on ezrin phosphorylation, an aliquot of affinity matrix was treated with λ-protein phosphatase (Sigma) followed by two washes to remove non-binding proteins. The proteins bound on affinity matrix were then eluted with 0.2 M glycine, pH 2.3) followed by 75% ethanol precipitation at −20 °C for 1 h. The precipitated proteins were then reconstituted in SDS-PAGE

sample buffer and subjected to electrophoresis and immunoblotting analyses.

Purification of Recombinant Ezrin Proteins—Recombinant wild type ezrin together its phospho-mimicking (S66D) and non-phosphorylatable (S66A) mutants were expressed in bacteria as histidine-tagged fusion proteins exactly as previously described (18). Purified ezrin was eluted with 250 mM imidazole and then applied to a gel filtration column to remove imidazole. The fusion protein was estimated to be 90–95% pure judged by SDS-PAGE; the major contaminants were degraded fragments of ezrin. Protein concentration was determined by Bradford assay.

Sample Preparation, Imaging, and Data Processing—Purified protein samples were diluted to 10 nM in Milli-Q water and placed on ice. 10 μl of protein sample was added onto a mica surface that had been pretreated with 10 mM spermidine. After 10 min the mica surface was gently washed with water and dried by nitrogen gas. The AFM imaging was performed on Nanoscope IIIa (Digital Instruments) with a type E scanner under the Tapping Mode^{TM} in air at room temperature. The AFM probes made of single silicon crystals with a cantilever length of 129 μm and a spring constant 33–62 newtons/m (Olympus) were used. Images were collected in height mode and stored in the 512 × 512-pixel format. The images obtained were then plane fitted and analyzed by the computer program accompanying the imaging module.

For the statistic analyses, 1 × 1-μm images were captured using the height mode in a 512 × 512 format. Thus, the AFM imaging provides images with subnanometer resolution. By measuring a contour length between two peaks of heads, we were able to get length between two heads of a single molecule.

For quantitative analyses, fitted Gaussian curves were overlaid on the histograms. The peaks of the distributions are indicated (mean ± S.D.). In general, >120 molecules per group were analyzed from three independent preparations.

[^{14}C]AP Uptake Assay—Stimulation of parietal cells was quantified using the AP uptake assay as previously described (19). Cells were transfected with siRNA 36 h before stimulation of histamine and isobutylmethylxanthine (100 and 30 μM, respectively). AP uptake values were normalized among the various preparations by expressing as a fraction of the stimulated control.

Immunofluorescence Microscopy—For cytolocalization of exogenously expressed ezrin, cultured parietal cells were transfected with wild type FLAG-ezrin and FLAG-ezrin phospho-mutants (S66A and S66D) and maintained in MEM for 30~36 h. Some cultures were treated with 100 μM cimetidine to maintain a resting state; others were treated with the secretory stimulants 100 μM histamine plus 50 μM isobutylmethylxanthine in the presence of SCH28080, a proton pump inhibitor (3). Treated cells were then fixed with 2% formaldehyde for 10 min and washed 3 times with PBS followed by permeabilization in 0.1% Triton X-100 for 5 min. Before application of primary antibody, the fixed and permeabilized cells were blocked with 0.5% BSA in PBS followed by incubation of primary antibodies against ezrin (4A5) or FLAG (M2; Sigma). The endogenous and exogenous ezrin proteins were labeled by a rhodamine-conjugated goat anti-mouse antibody and counterstained with GFP-Stx3. Coverslips were supported on slides by grease pencil markings and mounted in Vectorshield (Vector). Images were taken on a Zeiss Axiovert-200 fluorescence microscope using a 63 × 1.3 NA PlanApo objective. Figures were constructed using Adobe Photoshop.

Confocal Microscopy—Immunostained parietal cells were examined under a laser-scanning confocal microscope LSM510 NLO (Carl Zeiss, Jena, Germany) scan head mounted transversely to an inverted microscope (Axiovert 200; Carl Zeiss, Germany) with a 40 × 1.0 NA PlanApo objective. Single images were collected by an average of 10 scans at a scan rate of 1 s/scan. Optical section series were collected with a spacing of 0.4 μm in the Z-axis through the ~12-μm thickness of the cultured parietal cells. The images from double labeling were simultaneously collected using a dichroic filter set with Zeiss image processing software (LSM 5, Carl Zeiss). Digital data were exported into Adobe Photoshop for presentation.

Western Blot—Samples were subjected to SDS-PAGE on 6~16% gradient gel and transferred onto nitrocellulose membranes. Proteins were probed by appropriate primary antibodies and detected using ECL (Pierce). The band intensity was then quantified using a PhosphorImager (Amersham Bioscience).

RESULTS

Phosphorylation of Ezrin at Ser-66 Is Essential for Tubulovesicle Translocation to the Apical Plasma Membrane—Stx3 is present in the vesicular membrane fraction of gastric parietal cells (10, 21) and translocates to the apical membrane during parietal cell activation elicited by histamine (13, 20). In addition, ezrin is essential for tubulovesicle docking during parietal cell secretion via phosphorylation of Ser-66 (22). To delineate the molecular mechanism underlying the Stx3-mediated recruitment of H,K-ATPase-containing membrane to the apical membrane during the parietal cell activation, we performed affinity purification of the ezrin complex from the apical membrane-rich fraction from histamine-stimulated parietal cells. In histamine-stimulated parietal cells, H,K-ATPase-containing tubulovesicles are fused to the apical membrane as previously described (3).

As predicted, ezrin was recovered from the affinity isolation along with several major protein bands (Fig. 1*A*, *lane 2*). Because ezrin phosphorylation at Ser-66 occurs in histamine-stimulated parietal cell secretion, we sought to test if any of those associated proteins are dependent on ezrin phosphorylation at Ser-66. To this end, ezrin complex on affinity matrix was treated with λ-protein phosphatase followed by two washes to remove proteins liberated from ezrin dephosphorylation. As shown in Fig. 1*B*, *top panel*, *lane 3*), the phosphatase treatment eliminated ezrin phosphorylation at Ser-66 as judged by the Western blotting using phospho-Ser-66 ezrin specific antibody (*second panel*, *lanes 2* and *3*). Although the ezrin content remained unchanged in response to the phosphatase treatment (Fig. 1*B*, *top panel*, *lanes 2* and *3*), interestingly, the majority of the accessory proteins associated with phosphorylated ezrin were removed by phosphatase treatment (Fig. 1*A*, *lane 3*). Western blotting analysis confirmed that ACAP4, a protein bound to phosphorylated ezrin (22), is liberated from the affinity matrix after the phosphatase treatment (Fig. 1*B*, *third panel*, *lane 3*). As predicted, Stx3 is also liberated from the affinity matrix after the phosphatase treatment (Fig. 1*B*, *bottom panel*, *lane 3*). As a control, tubulin

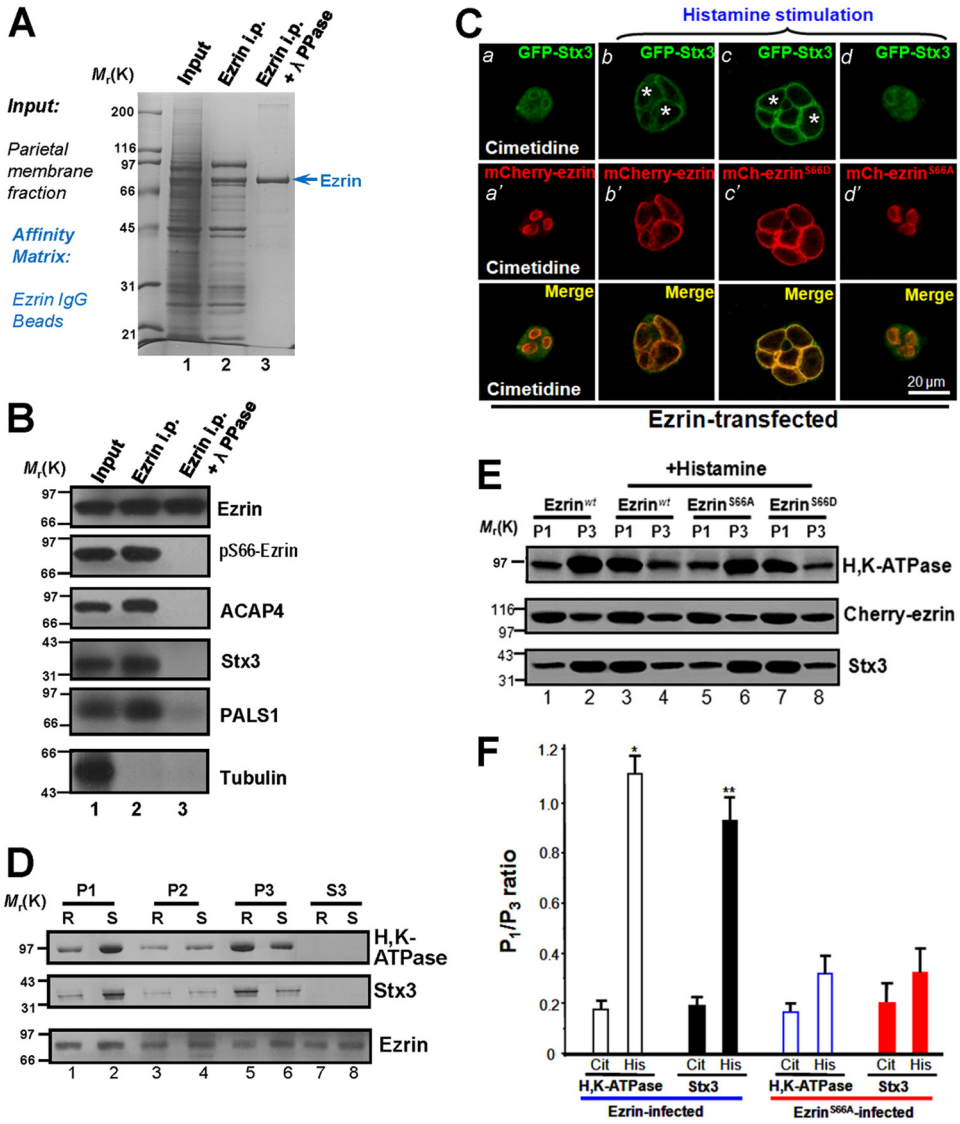

FIGURE 1. **Phosphorylation of ezrin at Ser-66 is essential for Stx3 and H,K-ATPase translocation to the apical plasma membrane.** *A* and *B*, the plasma membrane-enriched P1 fraction was extracted with TX-100, and the extract was incubated with ezrin antibody-conjugated beads as described under "Materials and Methods." The beads were washed successively with PBS before eluting ezrin with 0.2 M glycine, pH 2.3. All samples were separated by SDS gel electrophoresis. The proteins were either stained with Coomassie Blue (*A*) or transferred onto nitrocellulose membrane for Western blotting (*B*). Western blots were probed with an anti-ezrin antibody (*top panel*), anti-Ser(P)-66 antibody (*second panel*), anti-ACAP4 antibody (*third panel*), anti-Stx3 antibody (*fourth panel*), anti-PALS1 antibody (*fifth panel*), and anti-tubulin antibody (*bottom panel*). *i.p.*, immunoprecipitate; *λ PPase*, λ-protein phosphatase. *C*, this montage represents confocal images collected from resting and secreting gastric parietal cells doubly stained for GFP-Stx3 (*green*), mCherry-ezrin (*red*), and their merged images. Ezrin is mainly located in the apical plasma membrane of parietal cells (seen as *rings*) in a pattern suggestive of the apical plasma membrane invaginations that form the intracellular canaliculi (*b′*). Labeling of Stx3 is mainly located in the cytoplasm of parietal cells as they associate with tubulovesicle (*a′*), whereas a lesser degree of co-localization is seen in apical membrane. However, stimulation induces remodeling of the apical membrane, seen as a dilation of apical vacuoles in the parietal cells (*b′* and *c′*). Labeling of Stx3 is mainly located in the dilated apical vacuole membrane (*c*, *asterisk*), which is superimposed onto that of mCherry-ezrin distribution in the *Merge*. Note that histamine treatment maximally stimulates the dilation of apical vacuole membrane of mCherry-ezrin^{S66D}-expressing cells but failed to dilate apical vacuole membrane of mCherry-ezrin^{S66A}-expressing cells (*d′*). *Bar*, 15 μm. *D*, Western blotting analyses of ezrin, Stx3, and H,K-ATPase (α-subunit) of subcellular fractions derived from resting (*R*) and stimulated (*S*) gastric glands. Note that stimulation enriches the protein levels of H,K-ATPase and Stx3 in P_1 fraction. *E*, Western blotting analyses of ezrin, Stx3, and H,K-ATPase (α-subunit) of subcellular fractions derived from resting and stimulated gastric glands infected with mCherry-ezrin adenovirus (wild type, ezrin^{S66A}, and ezrin^{S66D}). *F*, quantification of the α-subunit of H,K-ATPase and Stx3 proteins from P_1 (plasma membrane-enriched) and P_3 (tubulovesicle-enriched) fractions. The measurements were expressed as P_1/P_3 ratio. All data are given as the means ± S.E. (*error bars*) of four preparations. *Cit*, cimetidine; *His*, histamine.

protein was not found in the ezrin immunoprecipitates, suggesting that the ezrin immunoprecipitation recovered proteins relatively specific for ezrin association.

To test if cellular distribution of Stx3 is responsive to the status of ezrin phosphorylation at Ser-66, cultured parietal cells were transiently transfect to express phospho-mimicking and non-phosphorylatable ezrin tagged with mCherry. Although GFP-Stx3 is primarily localized to cytoplasm of ezrin-expressing cells (Fig. 1*C*, *a′*), it becomes relocated to the apical plasma membrane in response to histamine stimulation (Fig. 1*C*, *b′*). Consistent with our speculation, expression of phospho-mimicking ezrin^{S66D} promotes Stx3 translocation to the apical membrane in histamine-stimulated parietal cells, whereas expression of non-phosphorylatable ezrin prevents the relocation of Stx3 to the apical membrane (Fig. 1*C*, *c′*), suggesting that ezrin phosphorylation at Ser-66 is functionally linked to Stx3 in parietal cell activation.

Because parietal cell activation is hallmarked by the translocation of H,K-ATPase from tubulovesicles to the apical membrane, we sought to assess the translocation of H,K-ATPase and Stx3 in non-phosphorylatable ezrin expression cells. To this end culture rabbit parietal cells were stimulated with histamine followed by subcellular fractionation and differentiated centrifugation as illustrated in Fig. 1*D*. A typical panel of Western blotting of subcellular fractionation was shown in Fig. 1*E* in which the histamine-stimulated relocation of an ~95-kDa polypeptide from the tubulovesicle fraction of P3 to apical plasma membrane fraction P1 was readily apparent (Fig. 1*E*, *top panel*; the α-subunit of H,K-ATPase contains >1000 amino acids but migrates as a band around 95-kDa due to its tight association with heavily glycosylated β-subunit). Stx3 is also redistributed to apical plasma membrane fraction P1 from the tubulovesicle fraction of P3 upon histamine stimulation (Fig. 1*E*, *middle panel*). To test if ezrin^{S66D} in involved in Stx3-mediated H,K-ATPase docking, we performed the aforementioned fractionation experiment using cultured parietal cells infected with adenoviral mCherry-ezrin (wild type, phospho-mimicking mutant, and non-phosphorylatable mutant) for 8 h followed by histamine stimulation. As shown in Fig. 1*F*, histamine-stimulated translocation of H,K-ATPase and Stx3 in wild type mCherry-ezrin-expressing cells exhibits an identical profile seen in uninfected cells (*e.g.* Fig. 1*E*). Interestingly, histamine failed to induce translocation of H,K-ATPase and Stx3 in non-phosphorylatable but not phospho-mimicking ezrin^{S66D}-infected cells, suggesting that ezrin phosphorylation at Ser-66 is critical for Stx3 docking to the apical plasma membrane. To quantify the translocation of Stx3 and α-subunit of H,K-ATPase in response to histamine stimulation, we carried out densitometric analyses of the α-subunit of H,K-ATPase and Stx3 proteins from P_1 (plasma membrane-enriched) and P_3 (tubulovesicle-enriched) fractions from resting and secreting rabbit gastric gland preparations and expressed the value as P_1/P_3 ratio. Quantification of the α-subunit of H,K-ATPase exhibits a characteristic translocation typically seen in histamine-stimulated secreting parietal cells (20). Statistical analyses from four different preparations demonstrate that Stx3 significantly translocates from cytoplasm to apical plasma membrane fraction in a pattern similar to that of H,K-ATPase in wild type and phospho-mimicking ezrin^{S66D}-expressing cells but not non-phosphorylatable ezrin^{S66A}-expressing cells (Fig. 1*F*, *, $p < 0.001$; **, $p < 0.001$ compared with those of cimetidine treatment).[6] We reason that ezrin$^{Ser\text{-}66}$ phosphorylation is essential for translocation of Stx3 and H,K-ATPase to the apical plasma membrane of secreting parietal cells.

Phosphorylation of Ser-66 on Ezrin Is Essential for Ezrin-Stx3 Interaction and Parietal Cell Acid Secretion—Our recent study showed that phosphorylation of ezrin at Ser-66 enables its association with ACAP4, an ARF6 GTPase-activating protein essential for acid secretion (22). To test if phosphorylated ezrin^{S66D} physically interacts with Stx3, we carried out a pulldown assay in which GST-fused Stx1–5 proteins on glutathione beads were used as the affinity matrix to bind MBP-ezrin^{S66D} protein. As shown in Fig. 2*A*, MBP-ezrin^{S66D} is only retained on the agarose beads immobilized with Stx3 (*lane 9*; *cyan arrow*), which was validated by an anti-ezrin Western blotting analysis (*bottom panel*). To validate the specificity of Stx3-ezrin^{S66D}, we carried out additional set of pulldown assays in which GST-Stx3 on glutathione beads was used as an affinity matrix to absorb purified recombinant protein MBP-ezrin^{S66D}, MBP-ezrin^{S66A} MBP-ezrin^{T567D}, and wild type MBP-ezrin (*lane 8*). As shown in Fig. 2*B*, only MBP-ezrin^{S66D} protein is bound on GST-Stx3 beads (*lane 6*), whereas MBP-ezrin^{S66A} and MBP-ezrin^{T567D} proteins remain in the solution (*lanes 1*, *3*, and *7*), suggesting that Stx3 binds to ezrin in a Ser-66 phosphorylation-dependent manner.

The specific Stx3-ezrin^{S66D} interaction *in vitro* suggests that they may form a complex essential for acid secretion. To this end we carried out ezrin immunoprecipitation using cell lysates from histamine-stimulated parietal cells. As shown in Fig. 2*C*, Stx3 forms a complex with ezrin in secreting parietal cells (*lane 8*). Immunoprecipitation of ezrin from non-secreting parietal cell lysates failed to pull down Stx3, validating the physiological relevance of ezrin-Stx3 interaction.

To map regions of Stx3 interacting with phospho-ezrin^{S66D}, we generated a series of deletion mutants of Stx3 fused with GST (Fig. 2*D*). The GST-fused Stx3 and its deletion mutants were used as an affinity matrix to bind histidine-tagged ezrin^{S66D}. As shown in Fig. 2*E*, the ezrin^{S66D} binding activity was mapped to the Habc domain of Stx3 (*lanes 3* and *4*). If the Habc domain of Stx3 interacts with ezrin upon its Ser-66 phosphorylation, the addition of an excess amount of Habc domain would interfere the association of endogenous Stx3 binding to ezrin and thereby inhibit parietal cell acid secretion. To test this hypothesis, the recombinant Habc domain of Stx3 (Stx3$^{1-147}$), the linker region of Stx3 (Stx3$^{147-180}$), and GST fusion protein were added to SLO-permeabilized glands in the presence and absence of cAMP/ATP as previously described (19, 20, 22). The addition of GST or GST-Stx3$^{147-180}$ caused relatively small changes in AP uptake (at most ~9% decrease), and there was no dose-dependent inhibitory effect. In contrast, the Habc domain caused a dose-dependent inhibition of acid secretion in SLO-permeabilized glands as measured by AP uptake. No significant inhibition was noted at 1 μg of protein/ml, but 5 μg of protein/ml caused a 27.3% reduction in acid secretion, and maximal inhibition (79 – 83%) occurred at 10 μg/ml (Fig. 2*F*). These experiments support the notion that the phospho-Ser-66-coupled ezrin-Stx3 interaction is required for parietal cell activation.

Single Molecule Imaging of Ezrin Unfolding in Response to Ser-66 Phosphorylation—The crystal structure reveals that the FERM domain has three compact lobes (15) in which Ser-66 resides. We speculate that phosphorylation of Ser-66 opens the compact lobes, which enables its association with Stx3. To probe the possible molecular conformation change of ezrin in response to Ser-66 phosphorylation, we carried out atomic force microscopic analyses using recombinant non-phosphorylatable (S66A) and phospho-mimicking (S66D) ezrin proteins. The recombinant proteins were produced in bacteria and purified to the homogeneity judged by SDS-PAGE (Fig. 3*A*). Fig. 3*B* represents typical AFM images seen in S66D ezrin preparations, whereas a magnified image was shown in Fig. 3*C*.

[6] H. Yu, X. Ding, and X. Yao, unpublished observations.

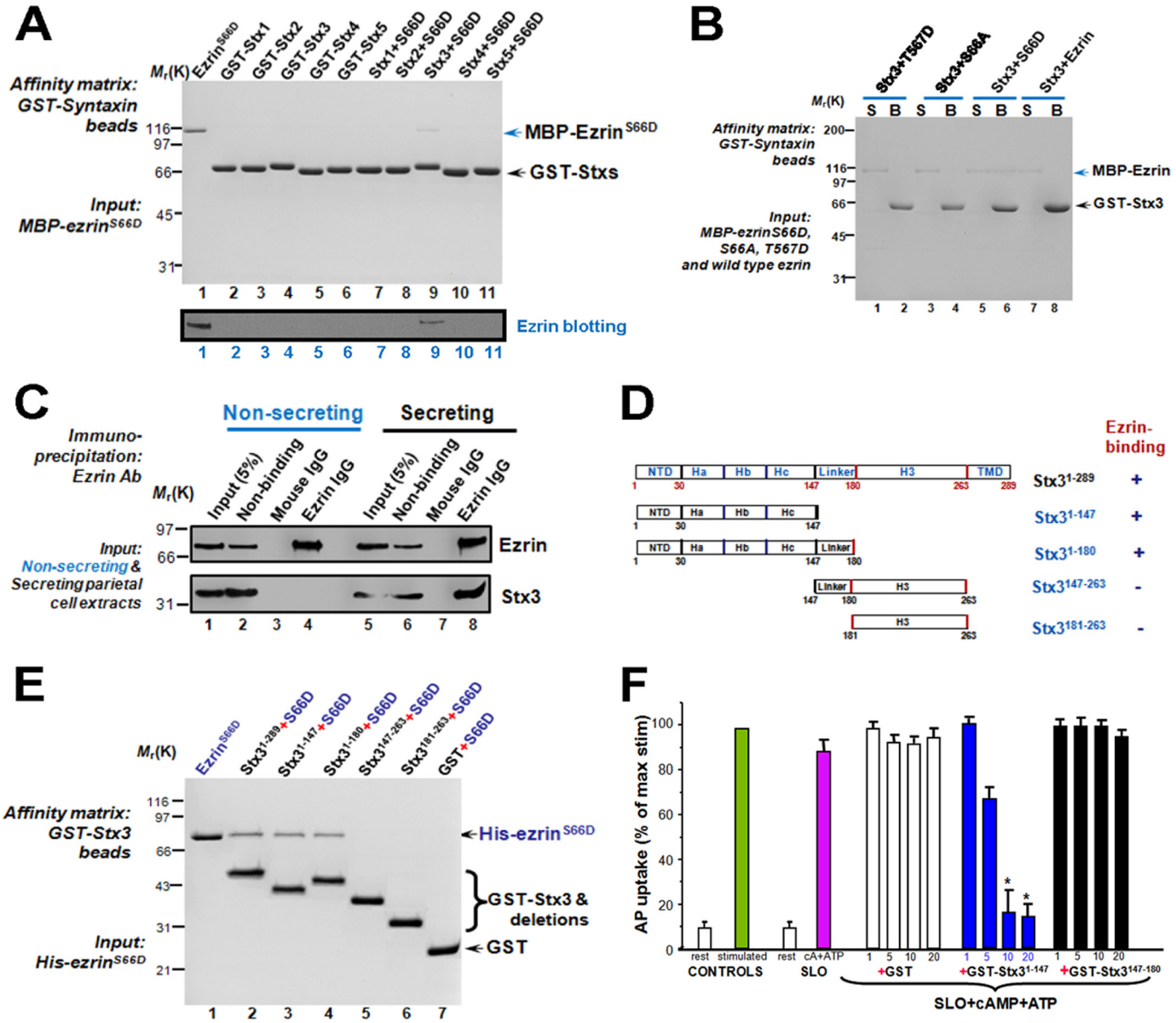

FIGURE 2. **Phosphorylation of Ser-66 on ezrin is essential for ezrin-Stx3 interaction and parietal cell acid secretion.** *A*, phosphorylation of Ser-66 of ezrin specifies its association with Stx3. Various GST-syntaxin proteins were purified on glutathione-Sepharose beads followed by incubation with MBP-ezrin^{S66D}. Beads were washed and boiled in SDS-PAGE sample buffer followed by SDS-PAGE analyses of proteins bound to the beads. Western blotting analyses shown on the *bottom panel* confirmed that Stx3 selectively binds to Ezrin^{S66D}. *B*, Stx3 specifically binds to ezrin^{S66D} but not ezrin^{S66A}, ezrin^{S567D}, or wild type ezrin. GST-Stx3 proteins were purified on glutathione-Sepharose beads followed by incubation with MBP-ezrin^{S66D}, MBP-ezrin^{S66A}, MBP-ezrin^{S567D}, or wild type ezrin proteins. Beads were washed and boiled in SDS-PAGE sample buffer followed by SDS-PAGE analyses of proteins bound to the beads. *R*, resting; *S*, stimulated. *C*, Stx3 forms a cognate complex with ezrin. Ezrin immunoprecipitation pulled down Stx3 from secreting parietal cells. *D*, diagram of Stx3 deletion mutants. *NTD*, N-terminal domain; *TMD*, terminal transmembrane domain. *E*, mapping the domains of Stx3 responsible for ezrin^{S66D} binding. Note the Habc domain of Stx3 binds to ezrin^{S66D}. *F*, Habc domain of Stx3 inhibits acid secretion in SLO-permeabilized gastric glands. Glands were SLO-permeabilized and incubated with various Stx3 deletion mutants before being stimulated with 100 μM cAMP plus 100 μM ATP, and the AP uptake was measured as described under "Materials and Methods." AP data are plotted as a percentage of the stimulated control for each experiment. *Error bars* represent S.E.; $n = 5$. *, significant difference from stimulated controls ($p < 0.001$).

We obtained images of individual recombinant ezrin proteins using scanning AFM as previously described (18). Scanning AFM revealed overall elongated structures with different lengths and heights. A crystallographic study shows that activated radixin exists as a linear structure with globular domains at both ends (23). As expected, a similar linear structure of ezrin was also enriched in phospho-mimicking ezrin (S66D; Fig. 3*C*), indicating that a conformational change of ezrin associated with its phosphorylation at Ser-66. The majority of ezrin^{S66D} protein exhibits a molecule structure as one head followed by a short tail. Given the heterogeneity, we measured the height of ezrin structures randomly selected to make unbiased histograms based on the measurement of 130 ezrin molecule structures. Our measurement indicates that heights of ezrin^{S66D} molecules fall into two categories with a majority of ezrin exhibiting a height of 0.48 nm (Fig. 3*D*; $n = 136$). On the other hand, majority of non-phosphorylatable ezrin^{S66A} molecule heights fall into one major category with an average of 0.54 nm (Fig. 3*E*; $n = 125$).

Our previous AFM study revealed an elongated structure of open molecular structure of ezrin^{T567D} with an overall length of

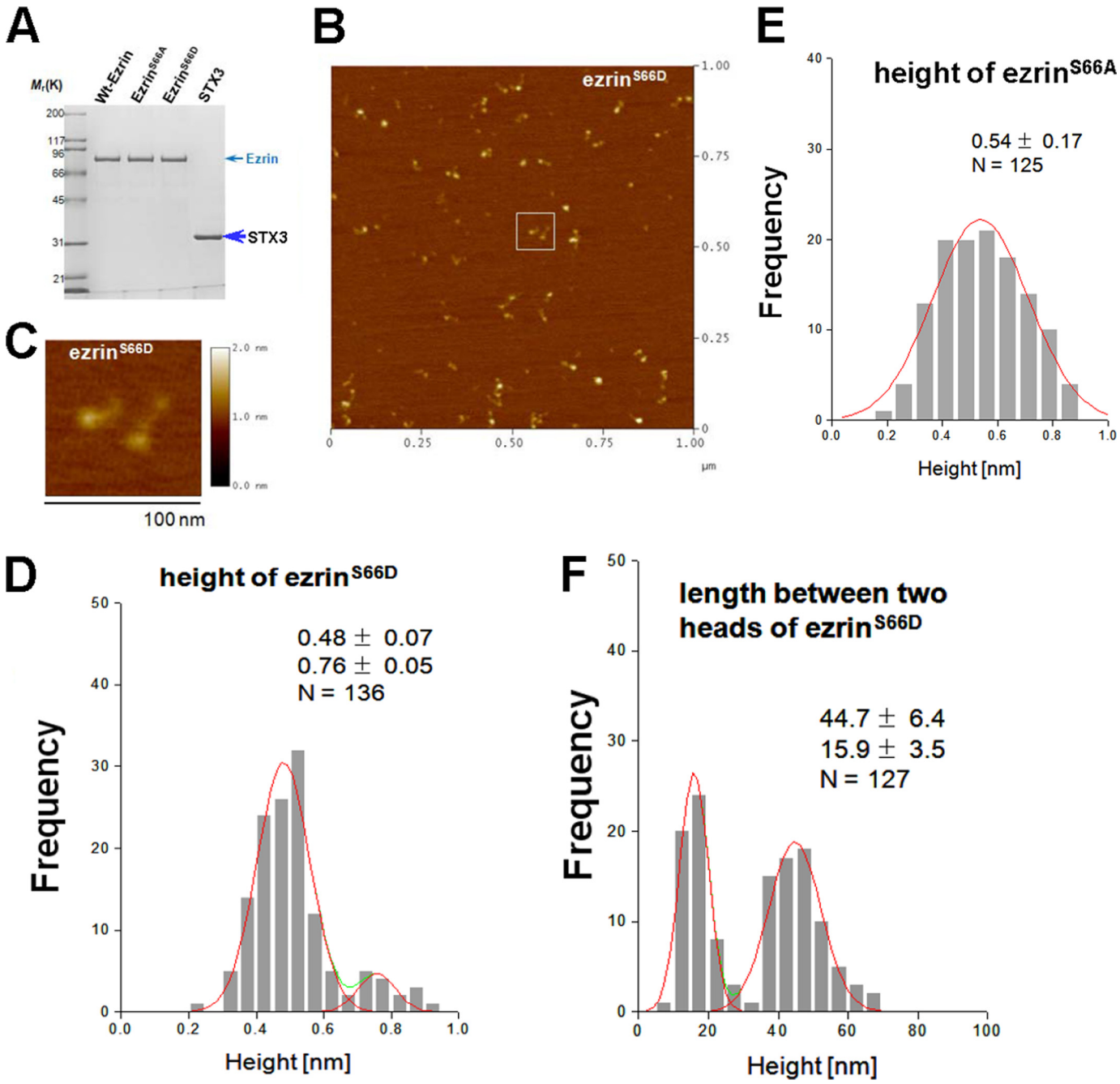

FIGURE 3. **Phosphorylation-coupled ezrin molecule unfolding revealed by AFM analyses.** *A*, recombinant ezrin^{S66A} and ezrin^{S66D} proteins were purified to homogeneity as determined by SDS-PAGE and stained by Coomassie Blue. *B*, AFM images of ezrin^{S66D} molecule structures (low magnification of broader view). Image size, 1000 × 1000 nm. *C*, magnified view of the *inset* in *B*. *Bar*, 100 nm. *D*, statistic histogram of single molecule height of ezrin^{S66D}. The major peak mean value is 0.48 nm, whereas a minor population show a mean height of 0.76 nm. Analyses were performed from a total of 136 measurements of three independent preparations. *E*, statistic histogram of single molecule height of ezrin^{S66A}. The major peak mean value is 0.54 nm. Analyses were performed from a total of 125 measurements of three independent preparations. *F*, statistic histogram of single molecule length of ezrin^{S66D}. The major length mean value is 44.7 nm, whereas a minor population shows a height of 15.9 nm. Analyses were performed from a total of 125 measurements of three independent preparations.

45 nm for fully open the ezrin molecule and an average of 15 nm for partially open the ezrin molecules (18). Statistic analysis indicated the length of ezrin^{S66D} falls into two populations with majority length of 44.7 nm (Fig. 3*F*; $n = 127$), suggesting that the majority of ezrin molecules become extended after phosphorylation at Ser-66. In contrast, the majority of ezrin^{S66A} molecules exhibit as half-closed monomers with the length of 15.9 nm as previously described for non-phosphorylatable ezrin^{T567A} (18). Together with previous analyses, we propose the phosphorylation of Ser-66 opens intramolecular N-C association and the three compact lobes of ezrin so its molecule structure of ezrin^{S66D} becomes extended.

Because Stx3 binds to ezrin in a Ser-66-phosphorylation-dependent manner, we reasoned that Stx3 recognizes a structure domain in the three compact lobes that becomes exposed upon Ser-66 phosphorylation. If this is indeed the case, incubation of

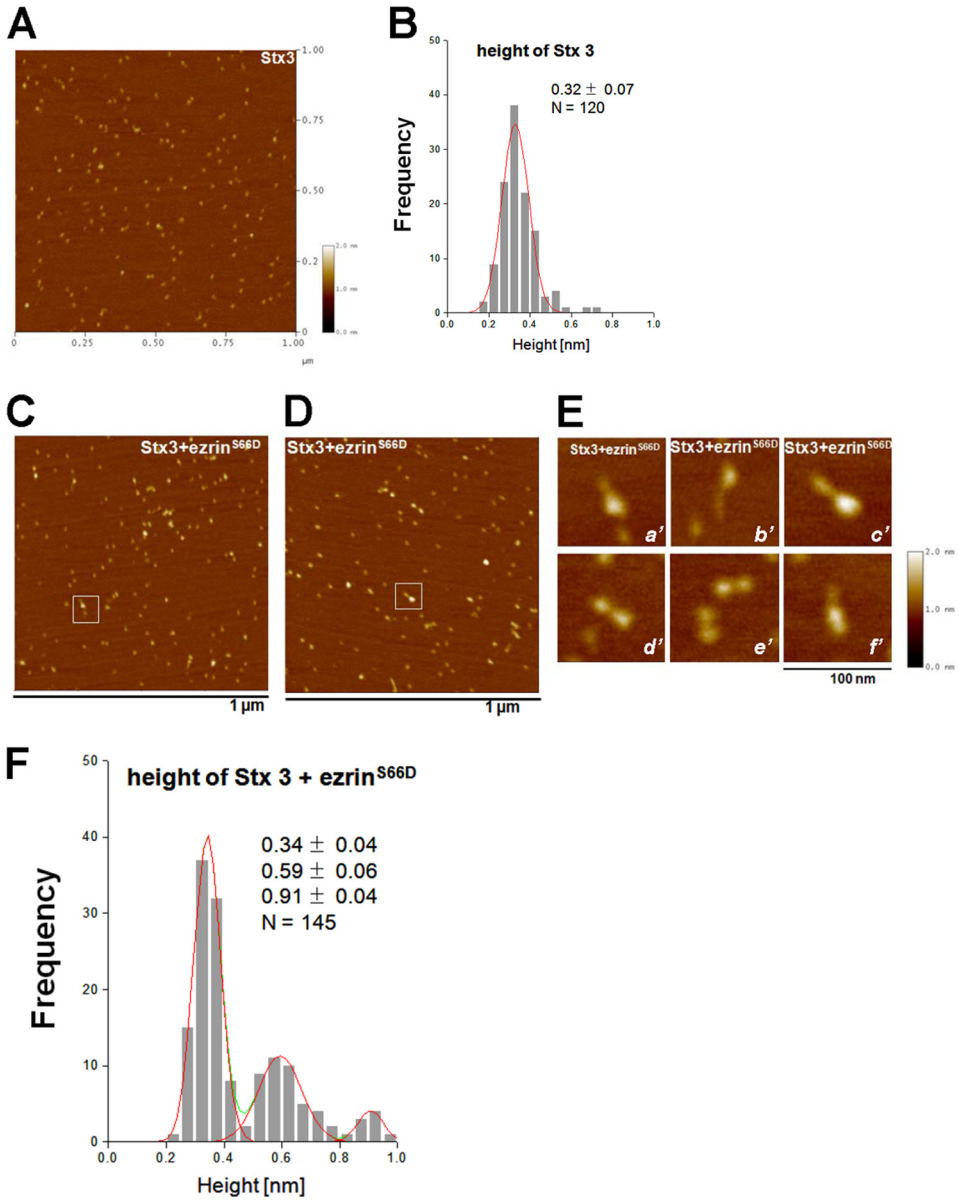

FIGURE 4. **Phosphorylation-coupled conformational change enables ezrin-Stx3 interaction.** *A*, representative molecule structures of Stx3. *B*, statistic histogram of single molecule mean height of Stx3. The major peak value is 0.32 nm from a total of 120 measurements of three independent preparations. *C*, representative molecule structures of Stx3 mixed with ezrin^{S66D}. *Bar*, 1 μm. *D*, representative molecule structures of Stx3 mixed with ezrin^{S66D} from a different preparation. *Bar*, 1 μm. *E*, magnified single molecule structure of Stx3 incubated with ezrin^{S66D}. *Bar*, 100 nm. *F*, statistic histogram of single molecule height of Stx3 incubated ezrin^{S66D}. There three major peak mean values: 0.34 nm (Stx3 alone), 0.59 nm (ezrin^{S66D} alone), and 0.91 nm (Stx3-bound ezrin^{S66D}). Representative magnified images were also shown from a total of 145 measurements of three independent preparations.

Stx3 with ezrin^{S66D} but not ezrin^{S66A} will result in an increase in ezrin molecule height. To this end we measured 120 molecules of Stx3 and revealed a major population mean height of 0.32 nm (Fig. 4, *A* and *B*). We next imaged and measured the heights of Stx3 in complex with ezrin^{S66D}. Two representative low magnification images of AFM were presented in Fig. 4, *C* and *D*, and magnified insets were presented in Fig. 4*E*. The majority of molecules exhibited a typical structure as one head followed by a short tail (Fig. 4*E*, *a*′, *b*′, and *c*′). In addition, a population of molecule exists as a linear structure with globular domains at both ends (Fig. 4*E*, *d*′, *e*′, and *f*′). Our measurement of 135 randomly selected molecules indicates that heights of molecules in the mixture of ezrin^{S66D} and Stx3 fall into three categories with a height of 0.34, 0.59, and 0.91 nm, respectively (Fig. 4*F*). The height of 0.34 nm represents free Stx3 molecules, whereas 0.59 nm represents the height of ezrin N-terminal globular head. The highest measure of 0.91 nm represents the binding of Stx3 on the top of N-terminal globular head. As a control, our measurement of 181 randomly selected molecules of ezrin^{S66A} mixed with Stx3 indicates no major change in the molecule height. Thus, we conclude that Ser-66 phosphorylation-induced conformation rearrangement of ezrin molecule enables ezrin-Stx3 complex formation.

DISCUSSION

Docking, the stable association of secretory vesicles with a specific zone of plasma membrane, is considered to be the necessary first step before vesicles gain fusion-competence, but it is

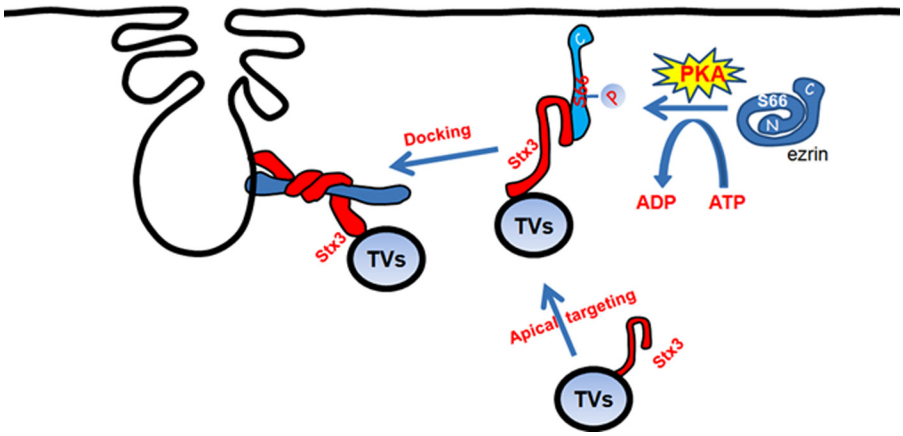

FIGURE 5. **Working model illustrates the histamine stimulation signaling induces ezrin conformational change that enables the association of ezrin with Stx3 and provides spatial cue for tubulovesicle translocation.** In non-secreting parietal cells Stx3 resides on tubulovesicle and relocates apically upon the histamine stimulation (*1*). Histamine stimulation induces PKA activation that phosphorylates ezrin at Ser-66 (*2*). Phosphorylation of Ser-66 elicits a conformational change of ezrin (*3*), which promotes docking of Stx3 at the apical membrane (*4*) for subsequent fusion of H,K-ATPase-containing vesicles to the apical membrane for proton pump (5).

unclear how vesicles dock in polarized secretion in response to hormone stimulation. Ezrin has been found essential for an array of dynamic membrane-cytoskeletal interaction underlying cell migration, immunological synapse formation, and polarized secretion (2, 24). Here we provide the first evidence that ezrin interacts with Stx3 in a conformation-oriented manner, and this interaction is essential for docking of H,K-ATPase containing tubulovesicles to the apical membrane. Stx3 binds to the extended three lobes of ezrin^{S66D} via its Habc domain, which could allow its H3 domain to form SNARE at same time. Thus, our data, therefore, provide direct evidence for a phosphorylation-coupled molecular switch of ezrin in orchestrating secretory vesicle docking and perhaps anchoring SNARE during regulated secretion in gastric parietal cells in response to histamine stimulation (Fig. 5).

Gastric ezrin was initially identified as a PKA substrate associated with parietal cell acid secretion (25). Both cellular and animal experiments demonstrated the essential role of ezrin in gastric acid secretion (8, 26). Our recent studies demonstrate that ezrin couples PKA-mediated phosphorylation to the remodeling of the apical membrane cytoskeleton associated with acid secretion in parietal cells (3). However, knowledge of how ezrin operates H,K-ATPase trafficking upon the parietal cell activation by histamine stimulation has remained elusive.

The SNARE hypothesis holds that membrane fusion involves the pairing of specific proteins in both the vesicle and target membranes. Despite the great importance of Stx3 in parietal cell acid secretion (12), the identities of the cognate partners that form a complex with Stx3 at the apical plasma membrane have remained elusive. Our present study shows that phospho-Ser-66 provides a spatiotemporal cue for tubulovesicle membrane trafficking to the apical membrane via a site-specific phosphorylation-coupled ezrin-Stx3 interaction. It is worth noting that ezrin is an interacting protein of the regulatory subunit of PKA that is implicated in the apical localization of PKA (27). Thus, the dynamic interaction between phospho-ezrin and Stx3 established here (see illustration in Fig. 5) together with a recently characterized ezrin-ACAP4 interaction (22) may organize an apical signaling, docking, and anchoring complex that orchestrates vesicular membrane recruitment and membrane cytoskeletal remodeling. Precise mapping of respective binding interfaces between the aforementioned proteins will aid in delineating the molecular mechanisms underlying polarity establishment and polarized secretion in gastric parietal cells. In fact, the recent development of super-resolution imaging-based delineation of protein-protein interaction interface in live cells will enable us to consolidate the dynamics of ezrin conformational changes and interaction with Stx3 illustrated in Fig. 5 into single parietal cell secretory dynamics (29). In addition, this newly developed nanoscale visualization of molecular dynamics will enable us to assess precisely the ezrin-Stx3 interaction dynamics during parietal cell activation in response to physiological stimuli and *Helicobacter pylori* toxins (19).

Phosphorylation of ezrin has been functionally linked to membrane dynamics and plasticity. Our previous study demonstrated that phosphorylation of the conserved Thr-567 residue of ezrin alters the physiology of gastric parietal cells (26) and participates in hepatocarcinoma metastasis (30). We recently established a protocol in which phosphorylation-mediated protein conformational change can be studied at the single molecule level using AFM (18). Using this protocol we correlated phosphorylation-induced conformational change of ezrin-Thr-567 with its functional activity in cellular localization. Using the same protocol, we show here that phosphorylation of ezrin at Ser-66 also unfolds ezrin intramolecular association. Although Thr-567 phosphorylation retains the N-terminal globular domain of ezrin half-folded (18), Ser-66 phosphorylation fully extends the ezrin molecule. Precise comparative analyses using photoactivation localization microscopy will provide a molecular illustration of phosphorylation-elicited functional activation of ezrin and delineate how phosphorylation-coupled protein conformational change is used as a signaling mechanism orchestrating cellular dynamics. Future work using a FRET-based sensor established for reporting substrate phosphorylation will help to illustrate the spatiotemporal gradient of ezrin phosphorylation in histamine-elicited parietal cell secretion and its relationship to the kinetics of

proton secretion (28), which will prompt the delineation of single molecule dynamics of polarized vesicle trafficking in gastric parietal cells.

Taken together, the present work reveals that phospho-ezrin interacts with Stx3 and specifies its apical localization. Finally, we show that disruption of ezrin-Stx3 interaction blocks the docking of the H,K-ATPase to the apical membrane and subsequent insertion of proton pump into the plasma membrane. We propose that the phosphorylation-coupled conformation change of ezrin provides a spatial control for H,K-ATPase docking at the apical membrane of gastric parietal cells.

Acknowledgments—We thank members of our groups for stimulating discussion.

REFERENCES

1. Yao, X., and Forte, J. G. (2003) Cell biology of acid secretion by the parietal cell. *Annu. Rev. Physiol.* **65,** 103–131
2. Bretscher, A., Edwards, K., and Fehon, R. G. (2002) ERM proteins and merlin: integrators at the cell cortex. *Nat. Rev. Mol. Cell Biol.* **3,** 586–599
3. Zhou, R., Cao, X., Watson, C., Miao, Y., Guo, Z., Forte, J. G., and Yao, X. (2003) Characterization of protein kinase A-mediated phosphorylation of ezrin in gastric parietal cell activation. *J. Biol. Chem.* **278,** 35651–35659
4. Nakamura, F., Amieva, M. R., and Furthmayr, H. (1995) Phosphorylation of threonine 558 in the carboxyl-terminal actin-binding domain of moesin by thrombin activation of human platelets. *J. Biol. Chem.* **270,** 31377–31385
5. Yao, X., Cheng, L., Rao, L., Han, B. G., and Forte, J. G. (1995) Biochemical characterization of ezrin-actin Interaction. *Mol. Biol. Cell* **6,** 140–140
6. Yao, X., Cheng, L., and Forte, J. G. (1996) Biochemical characterization of ezrin-actin interaction. *J. Biol. Chem.* **271,** 7224–7229
7. Hanzel, D. K., Urushidani, T., Usinger, W. R., Smolka, A., and Forte, J. G. (1989) Immunological localization of an 80-kDa phosphoprotein to the apical membrane of gastric parietal cells. *Am. J. Physiol.* **256,** G1082–G1089
8. Tamura, A. (2005) Achlorhydria by ezrin knockdown: defects in the formation/expansion of apical canaliculi in gastric parietal cells. *J. Cell Biol.* **169,** 21–28
9. Fasshauer, D., Antonin, W., Subramaniam, V., and Jahn, R. (2002) SNARE assembly and disassembly exhibit a pronounced hysteresis. *Nat. Struct. Biol.* **9,** 144–151
10. Peng, X. R., Yao, X., Chow, D. C., Forte, J. G., and Bennett, M. K. (1997) Association of syntaxin 3 and vesicle-associated membrane protein (VAMP) with H^+/K^+-ATPase-containing tubulovesicles in gastric parietal cells. *Mol. Biol. Cell* **8,** 399–407
11. Karvar, S., Yao, X., Duman, J. G., Hybiske, K., Liu, Y., and Forte, J. G. (2002a) Intracellular distribution and functional importance of vesicle-associated membrane protein 2 in gastric parietal cells. *Gastroenterology* **123,** 281–290
12. Karvar, S., Yao, X., Crothers, J. M., Jr., Liu, Y., and Forte, J. G. (2002b) Localization and function of soluble *N*-ethylmaleimide-sensitive factor attachment protein-25 and vesicle-associated membrane protein-2 in functioning gastric parietal cells. *J. Biol. Chem.* **277,** 50030–50035
13. Liu, Y., Ding, X., Wang, D., Deng, H., Feng, M., Wang, M., Yu, X., Jiang, K., Ward, T., Aikhionbare, F., Guo, Z., Forte, J. G., and Yao, X. (2007) A mechanism of Munc18b-syntaxin 3-SNAP25 complex assembly in regulated epithelial secretion. *FEBS Lett.* **581,** 4318–4324
14. Karvar, S., Zhu, L., Crothers, J., Jr., Wong, W., Turkoz, M., and Forte, J. G. (2005) Cellular localization and stimulation-associated distribution dynamics of syntaxin-1 and syntaxin-3 in gastric parietal cells. *Traffic* **6,** 654–666
15. Pearson, M. A., Reczek, D., Bretscher, A., and Karplus, P. A. (2000) Structure of the ERM protein moesin reveals the FERM domain fold masked by an extended actin binding tail domain. *Cell* **101,** 259–270
16. Smith, W. J., Nassar, N., Bretscher, A., Cerione, R. A., and Karplus, P. A. (2003) Structure of the active N-terminal domain of ezrin: conformational and mobility changes identify keystone interactions. *J. Biol. Chem.* **278,** 4949–4956
17. Hamada, K., Shimizu, T., Matsui, T., Tsukita, S., and Hakoshima, T. (2000) Structural basis of the membrane-targeting and unmasking mechanisms of the radixin FERM domain. *EMBO J.* **19,** 4449–4462
18. Liu, D., Ge, L., Wang, F., Takahashi, H., Wang, D., Guo, Z., Yoshimura, S. H., Ward, T., Ding, X., Takeyasu, K., and Yao, X. (2007) Single-molecule detection of phosphorylation-induced plasticity changes during ezrin activation. *FEBS Letters* **581,** 3563–3571
19. Wang, F., Xia, P., Wu, F., Wang, D., Wang, W., Ward, T., Liu, Y., Aikhionbare, F., Guo, Z., Powell, M., Liu, B., Bi, F., Shaw, A., Zhu, Z., Elmoselhi, A., Fan, D., Cover, T. L., Ding, X., and Yao, X. (2008) *Helicobacter pylori* VacA disrupts apical membrane-cytoskeletal interactions in gastric parietal cells. *J. Biol. Chem.* **283,** 26714–26725
20. Ammar, D. A., Zhou, R., Forte, J. G., and Yao, X. (2002) Syntaxin 3 is required for cAMP-induced acid secretion: streptolysin *O*-permeabilized gastric gland model. *Am. J. Physiol. Gastrointest. Liver Physiol.* **282,** G23–G33
21. Calhoun, B. C., and Goldenring, J. R. (1997) Two Rab proteins, vesicle-associated membrane protein 2 (VAMP-2) and secretory carrier membrane proteins (SCAMPs), are present on immunoisolated parietal cell tubulovesicles. *Biochem. J.* **325,** 559–564
22. Ding, X., Deng, H., Wang, D., Zhou, J., Huang, Y., Zhao, X., Yu, X., Wang, M., Wang, F., Ward, T., Aikhionbare, F., and Yao, X. (2010) Phospho-regulated ACAP4-ezrin interaction is essential for histamine-stimulated parietal cell secretion. *J. Biol. Chem.* **285,** 18769–18780
23. Ishikawa, H., Tamura, A., Matsui, T., Sasaki, H., Hakoshima, T., Tsukita, S., and Tsukita, S. (2001) Structural conversion between open and closed forms of radixin: low-angle shadowing electron microscopy. *J. Mol. Biol.* **310,** 973–978
24. Fehon, R. G., McClatchey, A. I., and Bretscher, A. (2010) Organizing the cell cortex: the role of ERM proteins. *Nat. Rev. Mol. Cell Biol.* **11,** 276–287
25. Dransfield, D. T., Bradford, A. J., Smith, J., Martin, M., Roy, C., Mangeat, P. H., and Goldenring, J. R. (1997) Ezrin is a cyclic AMP-dependent protein kinase anchoring protein. *EMBO J.* **16,** 35–43
26. Zhou, R., Zhu, L., Kodani, A., Hauser, P., Yao, X., and Forte, J. G. (2005) Phosphorylation of ezrin on threonine 567 produces a change in secretory phenotype and repolarizes the gastric parietal cell. *J. Cell Sci.* **118,** 4381–4391
27. Dransfield, D. T., Bradford, A. J., Smith, J., Martin, M., Roy, C., Mangeat, P. H., and Goldenring, J. R. (1997) Ezrin is a cyclic AMP-dependent protein kinase anchoring protein. *EMBO J.* **16,** 35–43
28. Chu, Y., Yao, P. Y., Wang, W., Wang, D., Wang, Z., Zhang, L., Huang, Y., Ke, Y., Ding, X., and Yao, X. (2011) Aurora B kinase activation requires survivin priming phosphorylation by PLK1. *J Mol. Cell. Biol.* **3,** 260–267
29. Xia, P., Liu, X., Wu, B., Zhang, S., Song, X., Yao, P.Y., Lippincott-Schwartz, J., and Yao, X. (2014) Super-resolution imaging reveals structural features underlying microtubule plus-end tracking. *Mol. Biol. Cell* 10.1091/mbc.E14-06-1133
30. Chen, Y., Wang, D., Guo, Z., Zhao, J., Wu, B., Deng, H., Zhou, T., Xiang, H., Gao, F., Yu, X., Liao, J., Ward, T., Xia, P., Emenari, C., Ding, X., Thompson, W., Ma, K., Zhu, J., Aikhionbare, F., Dou, K., Cheng, S. Y., and Yao, X. (2011) Rho kinase phosphorylation promotes ezrin-mediated metastasis in hepatocellular carcinoma. *Cancer Res.* **71,** 1721–1729